J Mater Sci (2008) 43:6556–6561
DOI 10.1007/s10853-008-2585-2

Characterization of cellular ceramics for high-temperature applications

W. Acchar · E. G. Ramalho · F. B. M. Souza · W. L. Torquato · V. P. Rodrigues · M. D. M. Innocentini

Received: 10 December 2007 / Accepted: 6 March 2008 / Published online: 17 September 2008

Abstract Polymeric sponge replication technique is the most used process to obtain ceramic foams with a cellular structure for filtration applications. This technique is based on an impregnation of a polymeric sponge with ceramic slurry, removal by squeezing, followed by burning out polymer and high temperature sintering. Ceramic filters must present high permeability and strength. However, these parameters are influenced in different ways by the processing method and the consequent cellular structure. In this work the relationship between permeability and strength has been investigated for 10- and 40-ppi (pores per linear inch) Al_2O_3–ZrO_2 filter materials. Characterization included the evaluation of the permeability and strength as well as the microstructural analyses of the fracture surface.

Introduction

Porous ceramics have been extensively investigated as structural materials for flow of fluids in high-temperature applications [1–3]. Ceramic porous structures are specially suitable for filtering molten metals, hot gases, thermal protection systems, and heat exchangers [4–8]. Materials for filtration at high temperatures must have special features: high permeability and mechanical strength at high temperatures. Morphology, size of the cell, and the degree of interconnectedness are fundamental parameters that strongly influence the application of these classes of materials [9–14]. Materials used as filters normally require an open cell structure. Permeability and filter strength are dependent on pore size and distribution. It is very difficult to optimize both properties because they are inversely proportional to each other. Mechanical strength generally decreases with increasing porosity, regardless of the permeability [11]. The final properties of these materials are a function of the processing method and the consequent microstructure [1–4, 12–14]. Several processing routes have been proposed for the production of ceramic porous material [1, 9–14]. The most widely spread industrial process to produce closed cell structure for filter application is the polymeric sponge replication method [13, 14]. This technique consists in dipping the polymer foam into a slurry containing an appropriate binder and the necessary ceramic materials, followed by a heat treatment that leads to the burning out of the organic elements and to the pressureless sintering at elevated temperatures of the ceramic skeleton [6]. Various ceramic materials such a cordierite, alumina, mullite can be used with this replica method [13, 14].

The objective of this work is to study the relationship between mechanical strength and permeability and also the fracture surface after strength tests of a commercial porous ceramic material (10 and 40 ppi) based on alumina +30 wt% ZrO_2 in order to classify the material as acceptable/adequate to be used as filter for hot gases applications.

W. Acchar (✉)
Department of Physics, Federal University of Rio Grande do Norte, Natal, RN CEP: 59072-970, Brazil
e-mail: acchar@dfte.ufrn.br

W. Acchar · E. G. Ramalho · F. B. M. Souza
Pos-graduation Program of Mechanical Engineering, Federal University of Rio Grande do Norte, Natal, RN, Brazil

W. Acchar · W. L. Torquato
Pos-graduation Program of Science and Materials Engineering, Federal University of Rio Grande do Norte, Natal, RN, Brazil

V. P. Rodrigues · M. D. M. Innocentini
Course of Chemical Engineering, University of Ribeirão Preto, UNAERP, Ribeirão Preto, SP, Brazil

Experimental procedure

Ceramic foams tested in this work were supplied by Minerfund Ltd., Ibaté-SP—Brazil, and were produced by making replicas of open-cell polyurethane foams with 10 and 40 pores per linear inch (ppi). Samples were disks with a diameter of 30 mm and about 10 mm thick. The total porosity of the samples (ε_{total}) was calculated based on mass and volume measurements using the expression $\varepsilon_{total} = 1 - \rho_g/\rho_s$, where ρ_g is the geometric sample density and ρ_s is the apparent density of the struts, obtained by the immersion method (Archimedes principle). The average pore size and the pore size distribution were evaluated through statistical analysis of images acquired with the help of a camera (*Galai CCD Macroviewer*) and processed using the software *Image-Pro Plus 3.0* at the Federal University of Sao Carlos (UFSCar). Permeability parameters were evaluated from airflow rate *versus* pressure drop measurements using the apparatus illustrated in Fig. 1. Permeability constants were fitted from Forchheimer's equation, expressed for flow of compressible fluids as:

$$\frac{P_i^2 - P_o^2}{2P_oL} = \frac{\mu}{k_1}v_s + \frac{\rho}{k_2}v_s^2 \quad (1)$$

where P_i and P_o are, respectively, the absolute air pressures at the entrance and exit of the sample; v_s is the superficial fluid velocity, determined by $v_s = Q/A$, where Q is the volumetric flow rate and A is the exposed surface area of the porous medium perpendicular to flow direction; L is the sample's thickness; μ is the air viscosity, and ρ is the air density, evaluated for $P_o = 716$ mmHg and $T = 25$–30 °C. The parameters k_1 and k_2 are known as Darcian and non-Darcian permeabilities, in reference to Darcy's law. They incorporate only the structural features of the porous medium and therefore are considered constant even when if the fluid or the flow conditions are modified. It is important to note that both parameters are dimensionally distinct: In SI units, k_1 is expressed in m^2, whereas k_2 is expressed in m. The first term of Forchheimer's equation [$\mu v_s/k_1$] represents viscous energy losses and prevails at low fluid velocities, while the quadratic term [$\rho {v_s}^2/k_2$] represents the kinetic energy losses and is more significant at higher velocities. The relative contribution of each term to the total pressure drop also depends on the values of k_1 and k_2, which can change significantly according to processing conditions. Therefore, the knowledge of the predominant relationship (linear or quadratic) for the pressure drop curve is critical for designing the best driving equipment for fluid flow in a given application. Permeability constants k_1 and k_2 were obtained in this work by fitting the experimental data of $[P_i^2 - P_o^2]/2P_oL$ *versus* v_s in Eq. 1, using the least-square method. At least 10 sets of P_i, P_o, and v_s values were acquired in a stationary airflow regime for each test.

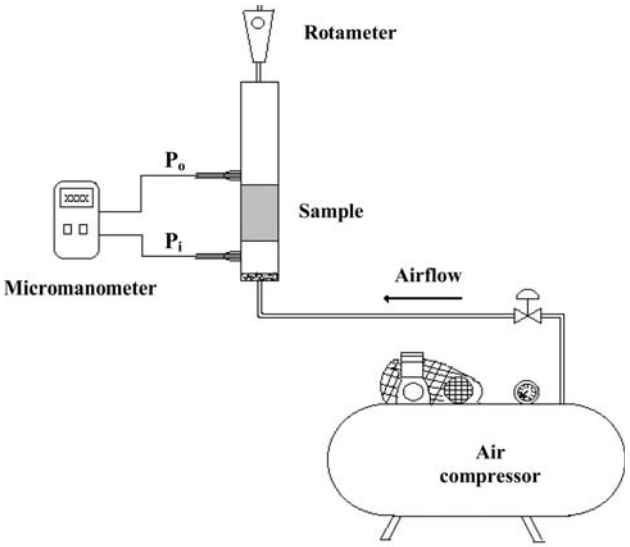

Fig. 1 Scheme of experimental rig for permeability evaluation of ceramic replicas

Samples of ceramic foams were cut into pieces of approximately 30 mm × 15 m × 10 mm using a diamond saw and subsequently submitted to mechanical tests. The mechanical strength of the samples (average of five bodies for each value) was measured using a universal testing machine (Zwick-Roell) in four-point bending test mode at a constant cross-head speed of 0.5 mm/min. The mechanical tests were performed at room temperature and also at 1,000 °C. Crystalline phases were identified by X-ray diffraction (Shimadzu XRD 600) in the 2θ range of 10–90° with a 2θ scanning rate of 2° min^{-1}. The cell geometry and the macrostructure of the ceramic foams were observed using an optical camera and the struts and the surface fracture were observed by a scanning electron microscope (Schimadzu).

Results and discussion

The main physical parameters obtained for 10- and 40-ppi ZiO_2 replicas are shown in Table 1. As expected, the sample

Table 1 Physical parameters obtained for ceramic foams tests in this work

Nominal pore counting (ppi)	k_1 (10^{-7} m^2)	k_2 (10^{-3} m)	ρ strut (g/cm^3)	ρ sample total (g/cm^3)	ε_{total} (−)	$d_{pore,\ optical}$ (mm)
10	9.41	6.18	3.06	0.52	0.829	2.33 ± 1.21
40	2.69	1.92	3.00	0.64	0.787	1.93 ± 1.06

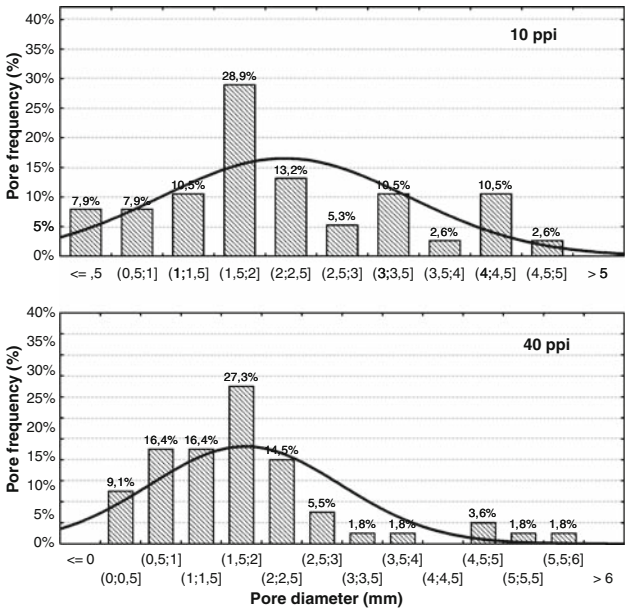

Fig. 2 Pore size distributions for 10- and 40-ppi replicas

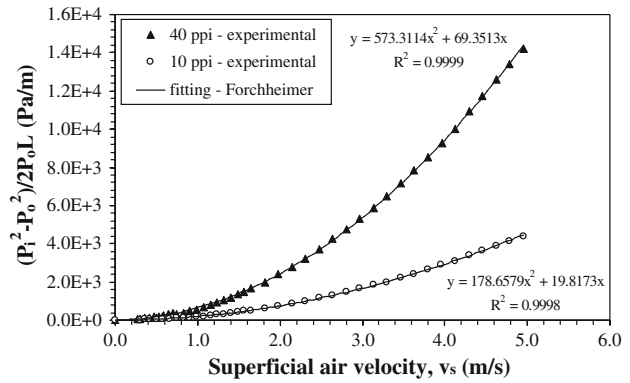

Fig. 3 Typical pressure drop curves obtained for 10- and 40-ppi replicas for airflow at room temperature

with lower pore count displayed slightly higher porosity, higher pore size, and higher permeability level. Treatment of data obtained from image analysis (Fig. 2) indicated that pore size distribution is different for both replicas and revealed that the 40-ppi sample displays smaller mean diameter. Figure 3 shows typical pressure drop curves in which permeability constants k_1 and k_2 are fitted. The parabolic trend of curves is confirmed by the exceptional correlation coefficient $R^2 = 0.999$, which implies that pressure drop is mostly ruled by the second term $[\rho v_s^2/k_2]$ of Eq. 1. Such correlation agreement was observed for all tested samples. This behavior is important because it proves that Darcy's law is not valid to predict pressure drop for such highly porous materials. The values for both constants are coherent with data presented in the literature (Fig. 4) and prove that ceramic replicas are among the most permeable rigid porous structures. The importance of parameters k_1 and

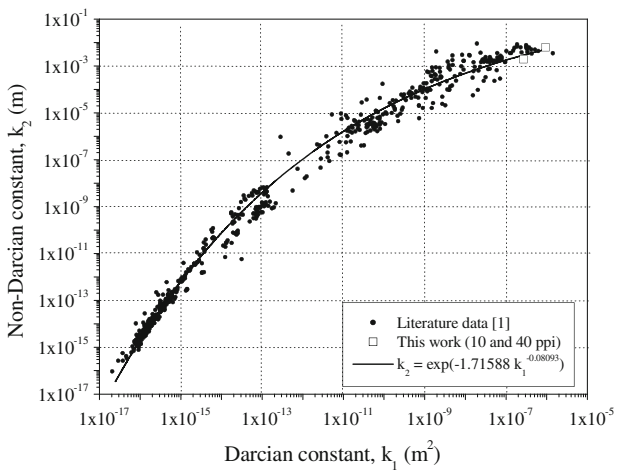

Fig. 4 Location of permeability data of ZiO_2 replicas tested in this work in a comprehensive data map available in the literature [1]

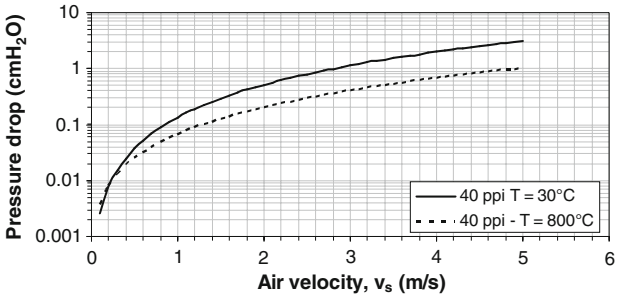

Fig. 5 Example of temperature effect on the pressure drop curve of a 40-ppi ZiO_2 replica. In this simulation, no correction was carried out on values of k_1 and k_2 constants obtained at room temperature (Table 1)

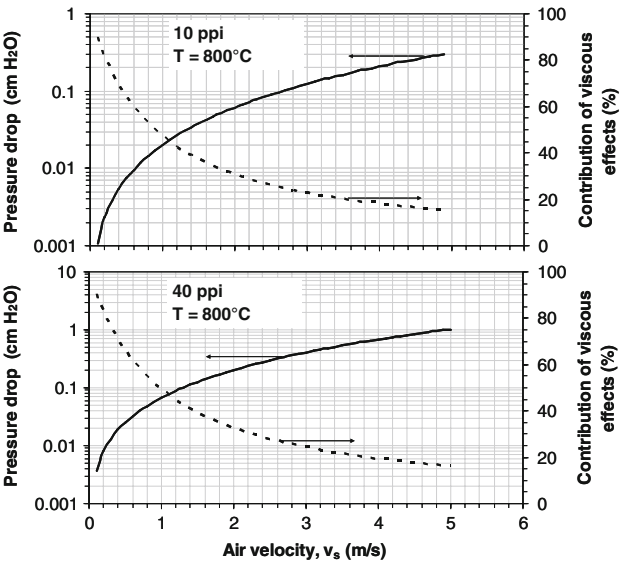

Fig. 6 Simulation of pressure drop curves with airflow at 800 °C and atmospheric pressure for 10- and 40-ppi ceramic replicas

k_2 is that they do not depend on the type of fluid or velocity range used for flow. Therefore, they are useful to predict the pressure drop for other applications, including those with flow at high temperatures, such as hot aerosol filtration and gas burning in boilers, incinerators, and power plants. In this situation, a variation in fluid properties (viscosity and density) is expected, which in turn affects the pressure drop curve in opposite ways. The increase in temperature causes an increase in gas viscosity but a decrease in gas density. Since inertial effects (the second term of Forchheimer's equation, $[\rho v_s^2/k_2]$) are dominant for replicas in typical operational velocities, then the prevailing effect will be a decrease in pressure drop (Fig. 5), i.e., less energy is lost during airflow and therefore savings in electric power with fans and blowers are possible. Nevertheless, it is worth noting that permeability constants k_1 and k_2 are also affected by temperature increase, since the structure is reversibly changed by thermal expansion effects. The literature has shown that in general, permeability constants increase with temperature [2–4], which implies that for high temperatures applications with gas flow, an even more pronounced decrease in pressure drop is expected for ceramic replicas.

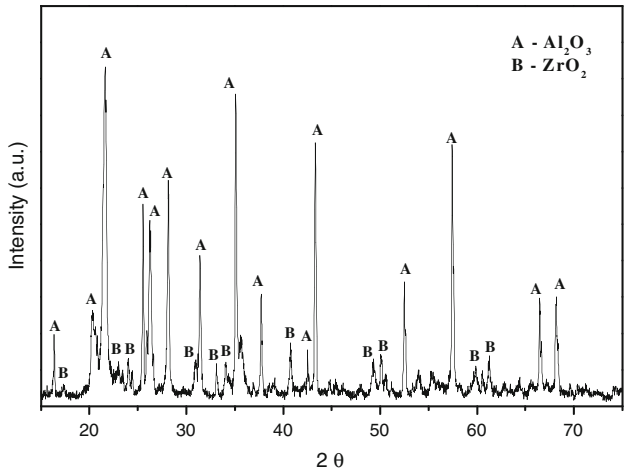

Fig. 7 X-ray diffraction pattern of the cellular cell investigated in this work

Figure 6 shows how the increase in gas velocity at high temperatures affects the contribution of inertial and viscous effects to pressure drop. The values of k_1 and k_2 for both 10- and 40-ppi samples were used to predict the pressure drop behavior during airflow at 800 °C and atmospheric pressure. It is clear according to this simulation that for higher velocity, the contribution of viscous effects is reduced. In practice, this also means higher turbulence inside the porous structure, which favors applications that involve mixing of fluids, such as in gas burners (oxygen and fuel).

Figure 7 shows the X-ray diffraction pattern of the ceramic foam. It can be noted that the ceramic foam is composed basically of alumina and zirconium oxide. Figure 8 shows the morphology of the ceramic foam with 10 and 40 ppi. Both ceramic foams have similar microstructure with the presence of some closed cells that are responsible for the degradation of the permeability behavior. It can be noted that an increase in porous density causes an increase in number of connections. The cell diameter decreases as the linear pore density increases from 10 to 40 ppi, as expected. The effect of cell size of the ceramic foam and the test temperature on the mechanical behavior is showed in Fig. 9. The low strength values observed for both materials are

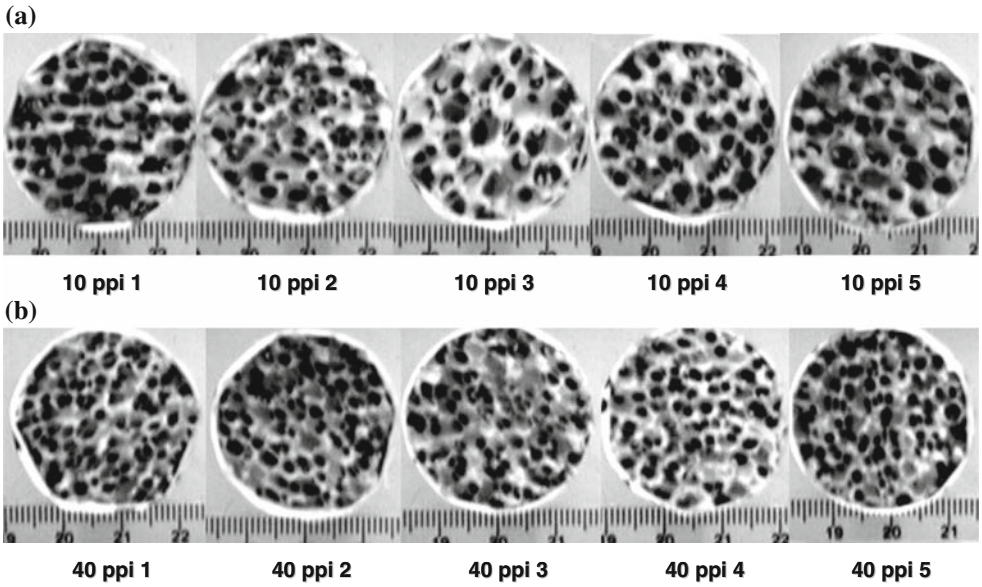

Fig. 8 Morphology of the ceramic foam with (**a**) 10 and (**b**) 40 ppi

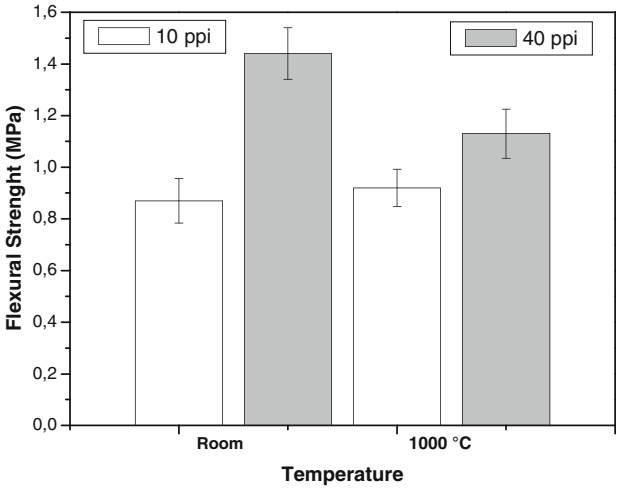

Fig. 9 Mechanical behavior of the ceramic foams

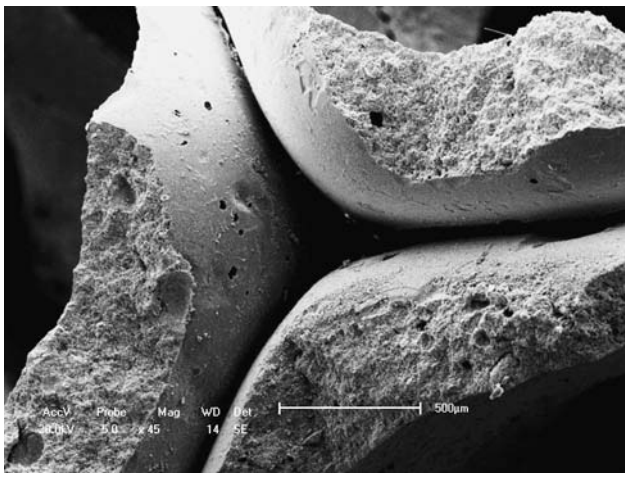

Fig. 11 Particle decohesion in the ceramic foam

associated with the presence of macro- and microdefects in the material such as triangular voids inside struts, internal microcracks between the filaments, and the fracture of the struts surface (Fig. 10). The high density of these macro- and microdefects facilitates crack propagation. Particle decohesions in the ceramic foam (Fig. 11), caused by an incomplete sintering of the ceramic grains that form the struts, are also responsible for the low mechanical performance. The results indicated that the material with 10 ppi did not present any significant influence on the resistance by increasing the test temperature. Strength values remain practically constant, ranging from 0.7 to 0.8 MPa. Contrary to that, the ceramic foam with 40 ppi shows a decrease in strength values from approximately 1.4–1.1 MPa. The higher flexural strength observed in the 40-ppi cell size can be attributed to the degree of compaction and the microcracks present in the filaments (struts). The number of the microcracks is proportional to the thickness of the struts. An increase in strut thickness, which occurs by decreasing the cell size from 40 to 10 ppi, causes probably an increase in microcracks, thus density, reducing the strength of the ceramic foam. Gibson and Ashby [14] have proposed a theoretical model for open-celled materials. This model consists of an array of cell struts and has shown that the

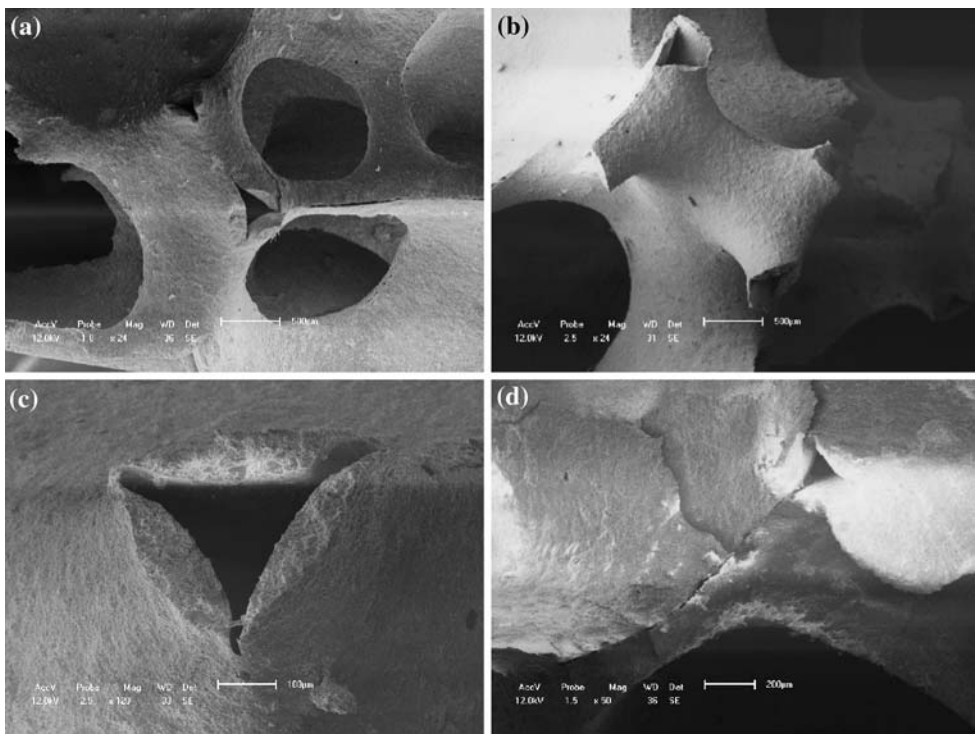

Fig. 10 SEM micrograph showing the presence of a microcrack between the filament and fracture surface of the filaments

mechanical behavior of the ceramic foam is determined mainly by the bending strength of the cell struts [13–15]. Based on this model it may be concluded that the strength of the ceramic foams investigated in this work can be improved by decreasing the macro- and microdefects found in the material (Fig. 8) and by densification of the cell walls.

Literature in the field of high temperature is still scarce. It is essential to understand this behavior especially in the case of hot filtration.

It must be pointed out that the permeability behavior and strength are two of the most important parameters to characterize ceramic foams. A compromise between these two parameters must be found to allow the use of porous ceramics as gas filters.

Studies are still underway to investigate the dependence of the mechanical behavior of the cellular ceramic materials on test temperatures and to determine the best relation between strength and permeability.

Conclusions

Two commercial ceramic foams with 10 and 40 ppi were analyzed. The results obtained in this work show that the main crystalline phases identified were alumina and zirconium oxide. The morphology of both materials is quite similar. The 10- and 40-ppi cell sizes have showed the presence of macrodefects (triangular voids) and microdefects (cracks and microspores). Strength and permeability have shown an inverse dependence, as expected. The 40- and 10-ppi cell sizes presented higher permeability and strength values, respectively. The best mechanical performance observed in the 40-ppi cell size can be attributed to the higher thickness of the filaments (struts).

Acknowledgement The authors would like to thank CNPq-CT-Petro for the financial support.

References

1. Innocentini MDM, Sepulveda P, Ortega FS (2005) In: Scheffler M, Colombo P (eds) Cellular ceramics: structure, manufacturing, properties and applications. Wiley-VCH Verlag GmbH, Weinheim, Germany, p 313
2. Rodrigues VP, Argiona LP, Pileggi RG, Romano RC, Coury JR, Innocentini MDM (2007) Permeability optimization of hot aerosol filters prepared from foaming of ceramic suspensions. In: 10th international conference and exhibition of the European ceramic society, 2007, Berlin-Alemanha. Anais do 10th international conference and exhibition of the European ceramic society
3. Freitas NL, Gonçalves JAS, Innocentini MDM, Coury JR (2006) J Hazard Mater B 316:747. doi:10.1016/j.jhazmat.2006.01.012
4. Innocentini MDM, Silva MG, Menegazzo BA, Pandolfelli VC (2001) J Am Ceram Soc 84(3):645
5. Gibosn LJ, Ashby MF (1999) Cellular solids, structure and properties, 2nd edn. Cambridge University Press, UK
6. Colombo P (2002) Key Eng Mater 1913:206
7. Gomez de Salazar JM, Barrena MI, Morales G, Matesanz L, Merino N (2006) Mater Lett 60:1687. doi:10.1016/j.matlet.2005.11.092
8. Montanaro L, Jorand Y, Fantozzi G, Negro A (1998) J Europ Ceram Soc 18:1339. doi:10.1016/S0955-2219(98)00063-6
9. Zhu X, Jiang D, Tan S (2002) Mater Res Bull 37:541. doi:10.1016/S0025-5408(02)00674-8
10. Sousa E, Silveira CB, Fey T, Greil P, Hotza D, Oliveira APN (2005) Adv Appl Ceram 104:1. doi:10.1179/174367605225011061
11. Romano RCO, Pandolfelli VC (2006) Cerâmica 52:213. doi:10.1590/S0366-69132006000200015
12. Moreira EA, Innocentini MDM, Coury JR (2004) J Europ Ceram Soc 24:3209. doi:10.1016/j.jeurceramsoc.2003.11.014
13. Innocentini MDM, Salvini VR, Pandolfelli VC (1999) Am Ceram Soc Bull 78:78
14. Scheffler M, Colombo P (2005) Cellular ceramics: structure, manufacturing, properties and applications. Wiley-VCH
15. Gibson LJ, Ashby MF (1983) Cellular solids: structure and properties. Cambridge University